High-Throughput and High-Port-Count Optical Cross-Connents Using Flexible Waveband Routing

Takuma Kuno
Department of Information and Communication Engineering
Nagoya University
Furo-cho, Chikusa, Nagoya,
464-8601 Japan
kuno.takuma@j.mbox.nagoya-u.ac.jp

Yojiro Mori
Department of Information and Communication Engineering
Nagoya University
Furo-cho, Chikusa, Nagoya,
464-8601 Japan
mori@nuee.nagoya-u.ac.jp

Suresh Subramaniam
Department of Electrical and Computer Engineering
The George Washington University
800 22nd Street NW SEH 6570,
Washington, DC 20052 USA
suresh@gwu.edu

Masahiko Jinno
Department of Engineering and Design
Kagawa University
2217-20 Hayashi-cho, Takamatsu,
761-0396 Japan
jinno@eng.kagawa-u.ac.jp

Hiroshi Hasegawa
Department of Information and Communication Engineering
Nagoya University
Furo-cho, Chikusa, Nagoya,
464-8601 Japan
hasegawa@nuee.nagoya-u.ac.jp

Abstract— Currently deployed optical cross-connects (OXCs) cannot support the large traffic expected in the near future because of the limited port count of wavelength-selective switches (WSSs). To resolve this problem, we proposed an OXC architecture that combines joint-switch WSSs and space switches. This OXC architecture realizes high port counts with low hardware cost in return for the additional insertion loss. However, the attainable maximum port count is still limited since the insertion loss increases with the port count. In this paper, we newly propose an OXC architecture whose insertion loss is constant irrespective of the port count. Consequently, the port count is virtually unlimited. Computer simulations show its low hardware cost and good routing performance. A proof-of-concept experiment evaluates the transmission performance, where the net throughput of 2.15 Pbps with port count of 84 is demonstrated.

Keywords—Optical-path network; Elastic optical network; Optical cross-connect; Wavelength-selective switch

I. INTRODUCTION

In optical-path networks, an optical cross-connect (OXC) can transport wavelength-division-multiplexed (WDM) signals without costly optical-electrical-optical conversion [1-4]. Now that traffic capacity of a single-mode fiber (SMF) is approaching the theoretical limit, space-division multiplexing (SDM) using a multi-core fiber (MCF) is being studied to overcome the capacity limit of SMFs [5-9]. The OXC of such systems must achieve high throughput and high port count so as to handle the large amounts of traffic expected [10-12]. The most widely deployed OXC consists of multiple wavelength-selective switches (WSSs) connected in the broadcast-and-select or route-and-select manner [13]; conventional OXC architectures cannot support a large number of ports as the number of costly WSSs needed increases super-linearly with the OXC port count [14]. Although spatially jointed switching can reduce the number of WSSs needed [15], it suffers from a severe routing restriction in that all signals with the same frequency in an incoming MCF must be switched to the same outgoing MCF. Another candidate, core-wise switching, virtually matches the routing performance of the non-restricted OXC [11]; however, a large number of WSSs are required. Given this background, we previously proposed an OXC architecture intended to achieve both low hardware cost and good routing performance [16]; it combines cost-effective joint-switch WSSs and delivery-and-coupling (DC) space switches. Thanks to the introduction of the DC space switches, WDM signals with the same wavelength in an incoming MCF can be delivered to different outgoing MCFs. Thus, the OXC architecture attains high routing performance while keeping the cost-effectiveness of spatially jointed switching. However, the insertion loss of the OXC increases with the OXC port count due to the insertion loss of the DC space switch. Consequently, this architecture cannot support the amounts of traffic expected.

In this paper, we propose a high-throughput and high-port-count OXC architecture that suits SDM-based networks, where joint-switch WSSs and DC space switches in a node are sparsely connected so as to keep the insertion loss acceptable. With such a scheme, the insertion loss of the OXC can be kept constant irrespective of the number of incoming/outgoing fibers. Although the sparse interconnection results in reduced routing flexibility, numerical simulations show that the penalty in fiber-utilization efficiency is less than 3% compared to core-wise switching. Transmission experiments successfully demonstrate the net OXC throughput of 2.15 Pbps and the OXC port count of 84 over the transmission distance of 700 km and node hop count of 7.

The remainder of this paper is organized as follows: Section II details the newly proposed OXC configuration; some previously reported OXC configurations are reviewed for the sake of comparison. In Section III, the hardware cost and routing performance are evaluated through network-design simulations. Section IV shows experimental results on transmission performance. Finally, this paper is concluded in Section V.

II. OPTICAL CROSS-CONNECT CONFIGURATIONS

Fig. 1(a) depicts the OXC architecture deployed in present SMF-based networks. The attainable port count of this OXC is bounded since the practical WSS port count is limited. Although cascading multiple WSSs can yield a high-port-count WSS, the number of costly WSSs needed increases super-linearly with the OXC port count [14]. Fig. 1(b) shows an OXC architecture based on spatially jointed switching [15], where the application to MCF-based networks is assumed. In return for its low hardware cost, the architecture suffers from the strict routing constraint that all signals with the same wavelength in an incoming MCF must be switched to the same outgoing MCF. As for Fig. 1(c), core-wise switching can deliver any WDM signal in core #i of an incoming MCF to core #i of any outgoing MCF. It was proven that the routing performance of core-wise switching is almost the same as that of non-restricted switching [11]; this node is realized by stacking relatively small-scale conventional-type OXCs consisting of multiple WSSs. Fig. 1(d) shows our previously proposed OXC using spatially-jointed flexible waveband routing [16]; it enables WDM signals with the same wavelength in an incoming MCF to be transported to different outgoing MCFs by using DC space switches consisting of optical selectors and couplers [17]. The OXC architecture offers low hardware cost because the DC space switch can be cost-effectively fabricated with planar-lightwave-circuit technologies or silicon-photonics technologies [18,19]. However, the insertion loss of the node increases with the OXC port count since the DC-switch scale must match the number of incoming/outgoing MCFs.

Fig. 2 illustrates the newly proposed OXC architecture for nN incoming M-core fibers and nN outgoing M-core fibers; *i.e.*, the OXC port count is nMN in terms of the number of cores. The OXC consists of nN M-array $1 \times B$ joint-switch WSSs, nN fan-in/out devices, nBM $N \times N$ DC space switches, nN M-array $B \times 1$ joint-switch WSSs, and nN fan-in/out devices, where n incoming/outgoing M-core fibers are virtually bundled. The routing operation is as follows: Optical paths in n-bundled M-core fibers are grouped into B wavebands by n M-array of $1 \times B$ joint-switch WSSs. As shown in Fig. 2, the grouping operations are homogeneous among all optical paths in the n-bundled M-core fibers. Each optical-path group in an M-core fiber is called a flexible waveband. The B wavebands are then delivered to mutually exclusive DC space switches. The DC space switches send each waveband to an M-array $B \times 1$ joint-switch WSS connected to the target n-bundled outgoing M-core fibers. The insertion loss of the OXC architecture is independent of the value of n even though the OXC scale is increased by the factor n. However, the routing flexibility is degraded since the number of selectable outgoing M-core fibers is reduced by $1/n$. The tradeoff between insertion loss and routing inflexibility can be arranged by adjusting the design parameter value n.
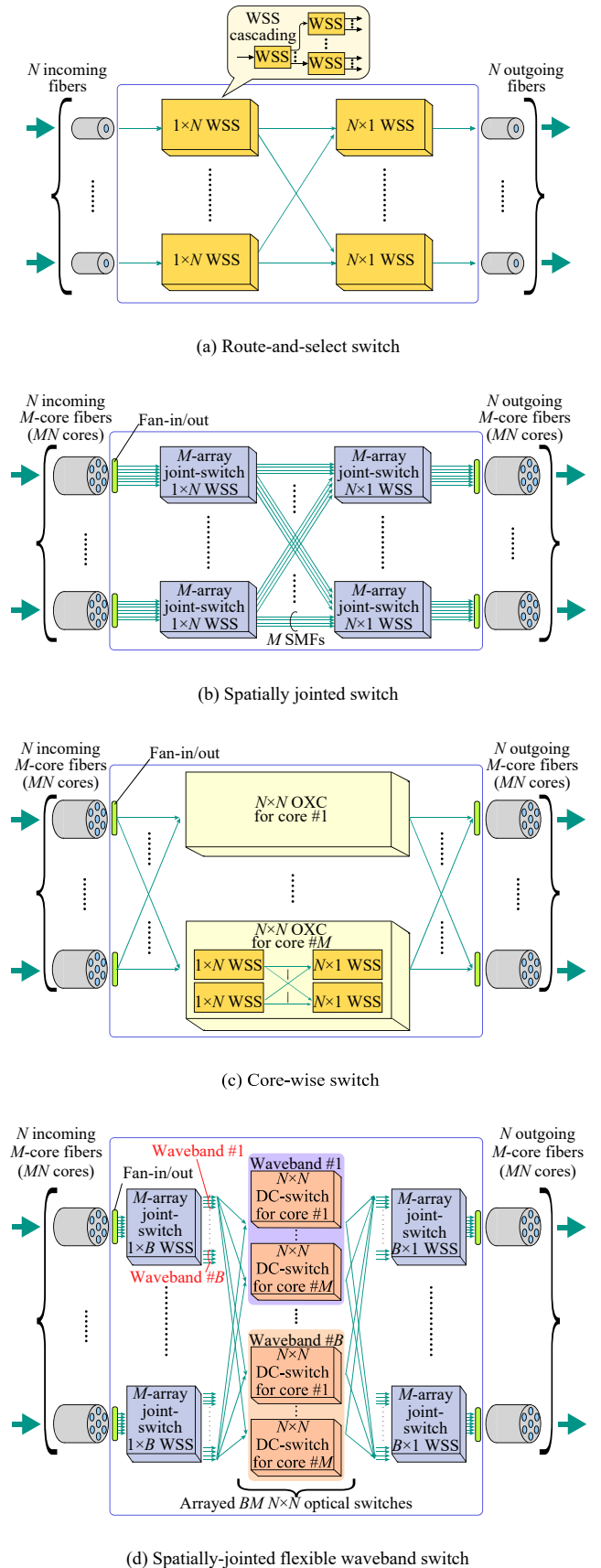

(a) Route-and-select switch

(b) Spatially jointed switch

(c) Core-wise switch

(d) Spatially-jointed flexible waveband switch

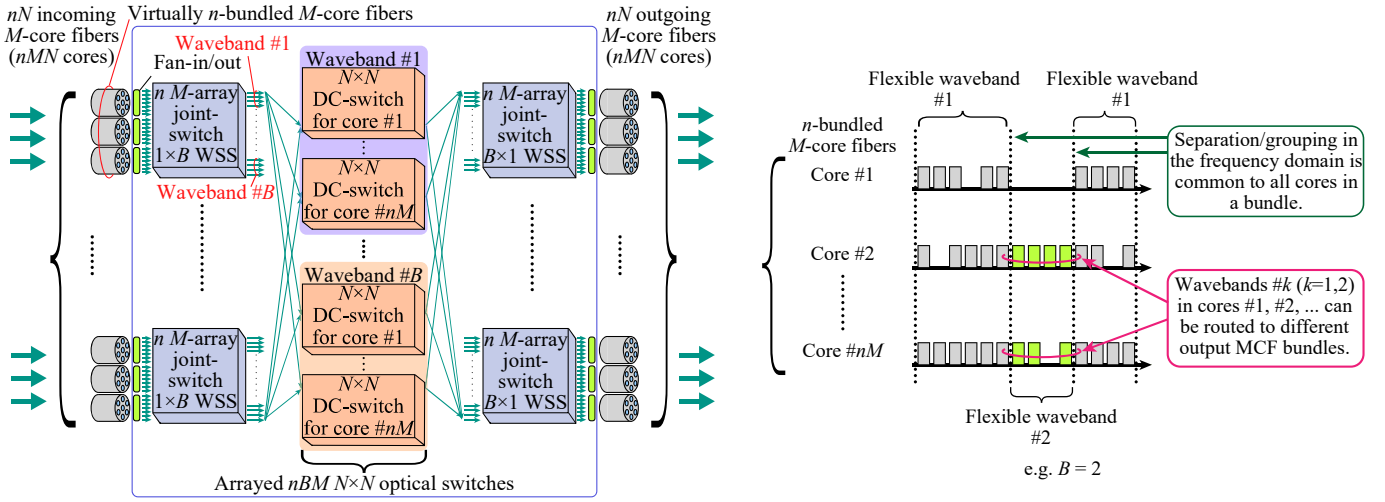Fig.1 Conventional OXC configurations.

Fig. 2 Proposed OXC architecture.

TABLE I. HARDWARE ASSESSMENT

		Route-and-select switching [13]	Spatially jointed switching [15]	Core-wise switching [11]	Spatially jointed flexible waveband switching [16]	Proposed scheme
Fiber type		Single-core fibers	M-core fibers	M-core fibers	M-core fibers	M-core fibers
Number of WSSs	1×(MK-1) WSSs	$2nMN\left\lceil\dfrac{nMN}{MK-1}\right\rceil$		$2nMN\left\lceil\dfrac{nN}{MK-1}\right\rceil$		
	M-array 1×(K-1) joint-switch WSSs		$2nN\left\lceil\dfrac{nN}{K-1}\right\rceil$		$2nN$	$2nN$
DC space switch	Size				$nN \times nN$	$N \times N$
	Number				BM	nBM

The OXC port count of $nMN \times nMN$ is considered, where the OXC port count is defined by the number of incoming/outgoing cores. Note that the implementation cost of a 1×(MK-1) WSS and that of an M-array 1×(K-1) joint-switch WSS are almost identical.

Table I summarizes the hardware cost of the proposed OXC architecture, where those for other OXC configurations are shown as references. Our scheme can offer much lower hardware requirements when the OXC port count is large.

It is noteworthy that our scheme can be applied to SMF-based networks because an M-core fiber and a bundle of M SMFs are functionally identical. In this case, fan-in/out devices are not necessary.

III. NETWORK SIMULATIONS

We evaluate the hardware cost and routing performance of the proposed OXC architecture shown in Fig. 2. The available bandwidth is 4.8 THz, *i.e.* 352 12.5 GHz frequency slots are utilized. Traffic demands are uniformly and randomly distributed. The traffic intensity is expressed by the average number of optical paths between each node pair. For each pair of traffic intensity value and node architecture, the number of fibers in a network is calculated 20 times and the results are averaged. We assume the use of two kinds of optical paths; 400 Gbps and 1 Tbps occupying 6 and 15 frequency slots, respectively. The path-occurrence probabilities of 400 Gbps and 1 Tbps are set to 2/5 and 3/5, respectively. Fig. 3 shows the three topologies tested; the 5×5 regular-mesh network, Japan network, and pan-European network [20,21]. Considering the use of commercially available devices, we examine 7-core fibers and 7-array joint-switch 1×B WSSs.

Fig. 4 plots the numbers of needed fibers versus traffic intensity. Here, the performance of core-wise switching is the baseline since its high routing performance are well proven [11]. The design parameter value n depicted in Fig. 2 is set to 3. When the topology is the 5×5 regular-mesh network, the penalty in the number of fibers needed is less than 2% if the number of wavebands B is set to ≥2. When B≥2, the performances are almost identical. Thus, the number of wavebands B is set to 2. Fig. 5 plots the numbers of needed WSSs versus traffic intensity; the results are normalized by those of spatially jointed switching because its cost effectiveness has been already demonstrated [15]. As for the 5×5 regular-mesh network, the number of WSSs demanded by our proposed architecture is 51% when the traffic intensity is 20. The other topologies demonstrate similar cost-effectiveness and high routing performance. It should be noted that our scheme necessitates DC space switches; however, the DC space switch can be cost-effectively implemented with planar-lightwave-circuit technologies or silicon-photonics technologies [18,19].

IV. TRANSMISSION EXPERIMENTS

We conducted experiments to evaluate the transmission performance of our OXC architecture. Due to the limited device availability, we used SMFs for the transmission links; however, similar results can be expected for MCF-based systems as discussed in Section II.

Fig. 6 illustrates the experimental setup. The 4.8 THz bandwidth in the C-band was fully utilized for WDM. At the transmitter side, a continuous wave (CW) was generated by a tunable laser. We selected the center frequency of the C-band as the target frequency to examine the worst condition in terms of fiber nonlinearity. A 16QAM signal was created by a lithium-niobate IQ modulator (IQM) driven by an arbitrary-waveform generator (AWG). After that, polarization-division multiplexing (PDM) was emulated by combining a polarization-beam splitter (PBS), a 10-ns-delay optical fiber, and a polarization-beam combiner (PBC). 64 CWs aligned with 75 GHz spacing were generated from 64 tunable lasers and combined in an optical coupler. The intensities of the CWs were modulated with a lithium-niobate intensity modulator (IM) driven by an 18.75 GHz cosine wave in the carrier-suppressed condition. This process yielded 128 CWs aligned with 37.5 GHz spacing. Then, we created 128-wavelength 200 Gbps DP-16 QAM signals by

using an IQM and a PDM emulator. WDM signal power was flattened by a gain-flattening filter (GFF) based on liquid crystal on silicon technology, while the frequency matching the target frequency was removed. After that, the target signal and non-target signals were combined by a 2×1 coupler. We thus obtained 128-subcarrier 200 Gbps DP-16QAM signals, *i.e.* 64-channel 400 Gbps dual-carrier DP-16QAM signals. After power optimization via an erbium-doped fiber amplifier (EDFA) and a variable optical attenuator (VOA), the signals entered a loop system. The loop system consisted of two synthesized loop-controlling switches (SWs), a 2×2 splitter, a 100 km SMF, an EDFA, the OXC under test, and an EDFA. The OXC consisted of a 7-array joint-switch 1×2 WSS, a 4×4 DC space switch with 1×4 selector and 4×1 coupler, and a 7-array joint-switch 2×1 WSS. The losses of the WSS and the DC space switch were 9 dB and 6.5 dB, respectively. The loss coefficient, nonlinearity coefficient, and dispersion parameter of the SMF were 0.18 dB/km, 1.5/W/km, and 16.5 ps/nm/km, respectively. The noise figure of EDFA was around 5 dB. After circulating the loop, the signals entered a 100 km SMF. Finally, the target signal was extracted by an optical tunable filter (TF) and detected by a digital coherent receiver. The signal was demodulated by digital signal processing that included polarization recovery, carrier-phase estimation, frequency estimation, and symbol decoding [22,23]. The port count was 84 as the design parameter n was 3 (*i.e.* n=3, M=7, and N=4 in Fig. 2) and the maximum net OXC throughput was 2.15 Pbps (*i.e.* 84×64×400 Gbps).

Fig. 7 shows BERs measured as a function of the transmission distance, where acceptable BER was set to $2.7×10^{-2}$ assuming the use of forward error correction (FEC) [24]. We observe that the 400 Gbps dual-carrier DP-16QAM signal could be transmitted over 700 km and 7 hops. This combination of transmission distance and hop count covers most metro-network applications. Please note that this proof-of-concept experiment considers the worst case where the signal encounters spectrum narrowing at every node traversal. If we apply an impairment-aware routing and spectrum assignment algorithm for the path-setup process, the maximum transmissible distance and hop count would be extended [25]. Furthermore, we can expect much wider-area applications by using QPSK signals as they are much more robust against transmission impairment.

(a) 5 × 5 regular mesh network   (b) Japan network [20]   (c) Pan-European network [21]
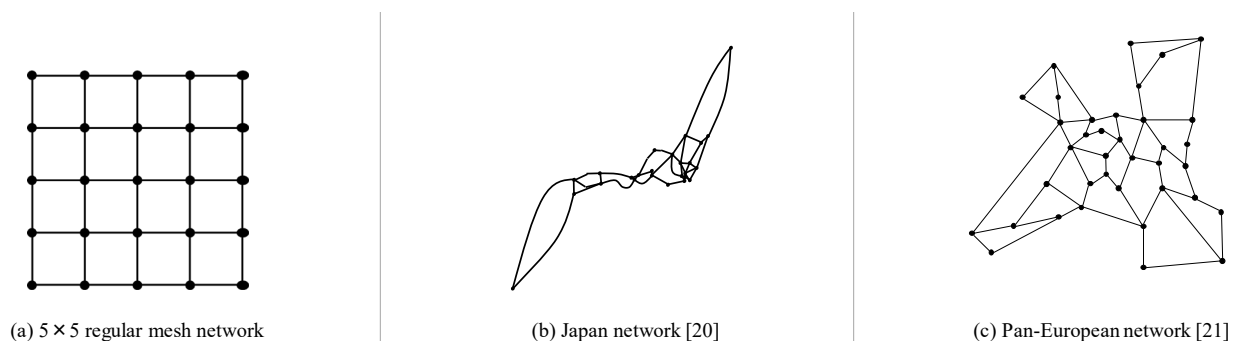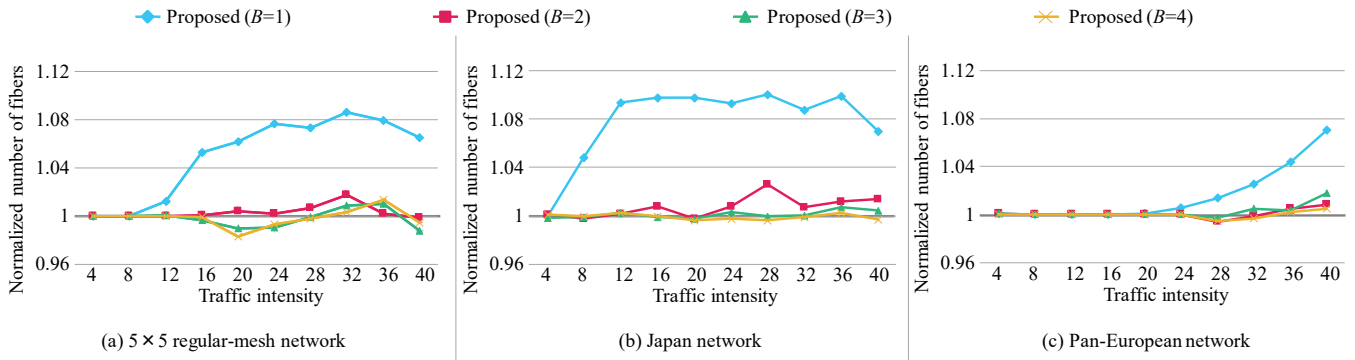
Fig. 3 The examined topologies.

Fig. 4 The number of needed fibers versus traffic intensity, where the results are normalized by those of core-wise switching [11]. Traffic intensity is defined by the average number of paths between each node pair. The design parameter n shown in Fig. 2 is set to 3.
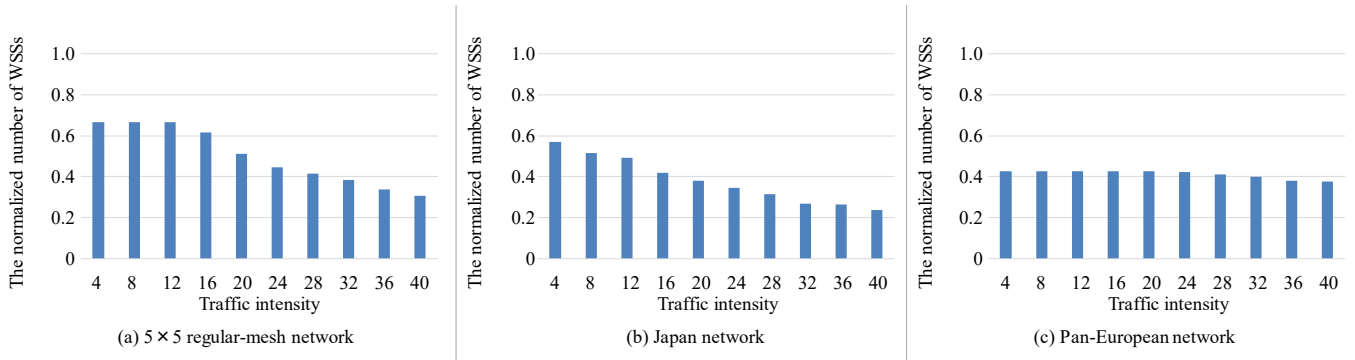

Fig. 5 The number of needed WSSs versus traffic intensity, where the results are normalized by those of the conventional spatially jointed switching [15]. Traffic intensity is defined by the average number of paths between each node pair. The design parameter n shown in Fig. 2 is set to 3.

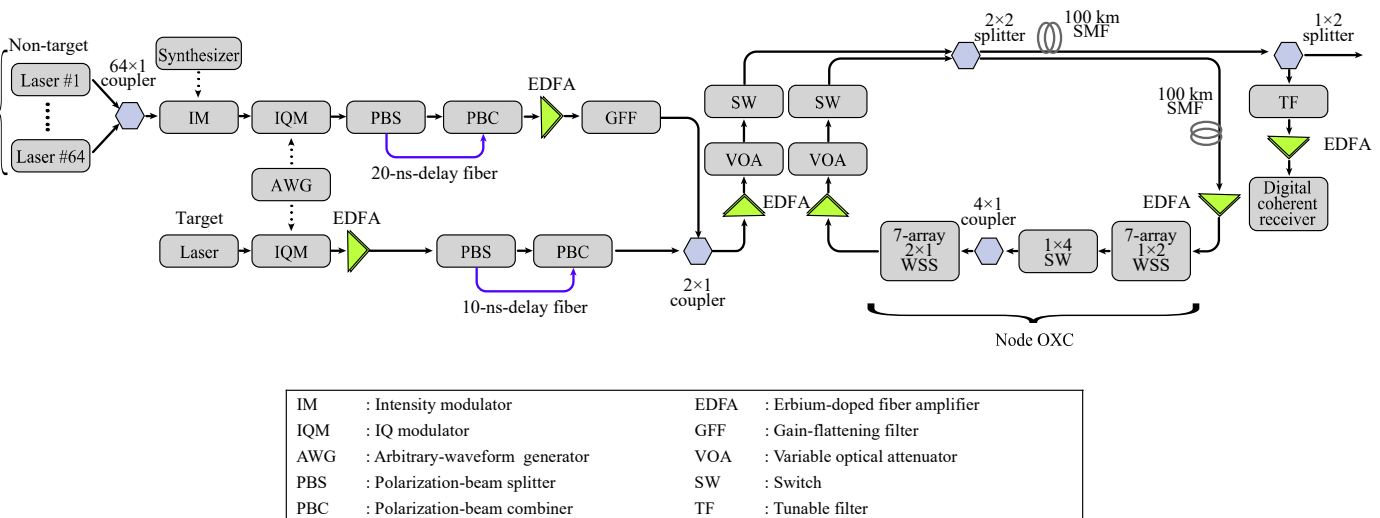| IM | : Intensity modulator | EDFA | : Erbium-doped fiber amplifier |
IQM	: IQ modulator	GFF	: Gain-flattening filter
AWG	: Arbitrary-waveform generator	VOA	: Variable optical attenuator
PBS	: Polarization-beam splitter	SW	: Switch
PBC	: Polarization-beam combiner	TF	: Tunable filter

Fig. 6. Experimental setup, where 64-channel 400 Gbps dual-carrier DP-16QAM signals were multiplexed in the full C-band.
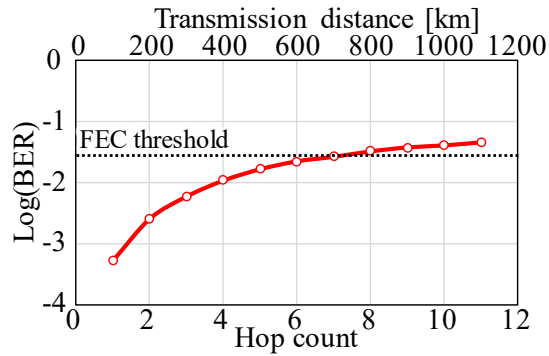
Fig. 7. Measured BERs versus transmission distance or hop count.

V. CONCLUSION

We proposed a high-throughput and high-port-count OXC architecture comprising joint-switch WSSs and DC space switches. The sparse interconnection among joint-switch WSSs and DC space switches can keep the OXC insertion loss small irrespective of the OXC port count. Consequently, the OXC architecture can be expanded in a highly scalable manner. Network simulations confirmed its low hardware cost and good routing performance. Transmission experiments demonstrated that our OXC architecture achieved 700 km transmission of 400 Gbps dual-carrier DP-16QAM signals over 7 hops. The maximum net throughput of 2.15 Pbps and the port count of 84 were attained.

REFERENCES

[1] A. Watanabe, S. Okamoto, and K. Sato, "Optical Path Cross-Connect Node Architecture with High Modularity for Photonic Transport Networks," IEICE Transactions on Communications, Vol. E77-B, No.10, pp.1220-1229 (1994).

[2] J. Strand and A. Chiu, "Realizing the Advantages of Optical Reconfigurability and Restoration with Integrated Optical Cross-Connects," IEEE/OSA Journal of Lightwave Technology, vol. 21, issue 11, pp. 2871-2882 (2003).

[3] M. Jinno, H. Takara, B. Kozicki, Y. Tsukishima, Y. Sone, and S. Matsuoka, "Spectrum-Efficient and Scalable Elastic Optical Path Network: Architecture, Benefits, and Enabling Technologies," IEEE Communications Magazine, vol. 47, issue 11. pp. 66-73 (2009).

[4] R. Hashimoto, S. Yamaoka, Y. Mori, H. Hasegawa, K. Sato, K. Yamaguchi, K. Seno, and K. Suzuki, "First Demonstration of Subsystem-Modular Optical Cross-Connect Using Single-Module 6 × 6 Wavelength-Selective Switch," IEEE/OSA Journal of Lightwave Technology, vol. 36, issue 7, pp. 1435-1442 (2018).

[5] D. J. Richardson, J. M. Fini, and L. E. Nelson, "Space-Division Multiplexing in Optical Fibres," Nature Photonics vol. 7, pp. 354-362 (2013).

[6] G. Li, N. Bai, N. Zhao, and C. Xia, "Space-Division Multiplexing: the Next Frontier in Optical Communication," OSA Advances in Optics and Photonics, vol. 6, issue 4, pp. 413-487 (2014).

[7] G. M. Saridis, D. Alexandropoulos, G. Zervas, and D. Simeonidou, "Survey and Evaluation of Space Division Multiplexing: From Technologies to Optical Networks," IEEE Communications & Tutorials vol. 17, issue 4, pp. 2136-2156 (2015).

[8] P. J. Winzer, "Scaling Optical Fiber Networks: Challenges and Solutions," OSA Optics and Photonics News, vol. 26, pp. 28-35 (2015).

[9] D. Soma, Y. Wakayama, S. Beppu, S. Sumita, T. Tsuritani, T. Hayashi, T. Nagashima, M. Suzuki, M. Yoshida, K. Kasai, M. Nakazawa, H. Takahashi, K. Igarashi, I. Morita, and M. Suzuki, "10.16-Peta-B/s Dense SDM/WDM Transmission Over 6-Mode 19-Core Fiber Across the C+L Band," IEEE/OSA Journal of Lightwave Technology, vol. 36, issue 6, pp. 1362-1368 (2018).

[10] D. M. Marom, P. D. Colborne, A. D'errico, N. K. Fontaine, Y. Ikuma, E. Proietti, L. Zong, J. M. Rivas-Moscoso, and L. Tomkos, "Survey of Photonic Switching Architectures and Technologies in Support of Spatially and Spectrally Flexible Optical Networking," IEEE/OSA Journal of Optical Communications and Networking, vol. 9, issue 1, pp. 1-26 (2017).

[11] F.-J. Moreno-Muro, R. Rumipamba-Zambrano, P. Pavon-Marino, J. Perello, J. M. Gene, and S. Spadaro, "Evaluation of Core-Continuity-Constrained ROADMs for Flex-Grid/MCF Optical Networks," IEEE/OSA Journal of Optical Communications and Networking, vol. 9, issue 11, pp. 1041-1050 (2017).

[12] G. Rizzelli, G. Maier, M. Quagliotti, M. Schiano, and A. Pattavina, "Assessing the Scalability of Next-Generation Wavelength Switched Optical Networks," IEEE/OSA Journal of Lightwave Technology, vol. 32, issue 12, pp. 2263-2270 (2014).

[13] S. L. Woodward, M. D. Feuer, and P. Palacharla, "ROADM-Node Architectures for Reconfigurable Photonic Networks," in *Optical Fiber Telecommunications Volume VIB Sixth Edition: Systems and Networks*, Academic Press (2013).

[14] M. Niwa, Y. Mori, H. Hasegawa, and K. Sato, "Tipping Point for The Future Scalable OXC: What Size MxM WSS Is Needed?," IEEE/OSA Journal of Optical Communications and Networking, vol. 9, issue 1, A1-A25 (2017).

[15] L. E. Nelson, M. D. Feuer, K. Abedin, X. Chou, T. F. Taunay, J. M. Fini, R. Issac, R. Harel, G. Cohen, and D. M. Marom, "Spatial Superchannel Routing in a Two-Span ROADM System for Space Division Multiplexing," IEEE/OSA Journal of Lightwave Technology, vol. 32, issue 4, pp. 783-789 (2013).

[16] H. Hasegawa, S. Subramaniam, and M. Jinno, "Node Architecture and Design of Spatially Jointed Flexible Waveband Routing Optical Networks," in Proc. of European Conference on Optical Communication (ECOC), paper Th.1.A.P63 (2019).

[17] M. Koga, A. Watanabe, T. Kawai, K. Sato, and Y. Ohmori, "Large-Capacity Optical Path Cross-Connect System for WDM Photonic Transport Network," IEEE Journal on Selected Areas in Communications, vol. 16, issue 7, pp. 1260-1269 (1998).

[18] T. Watanabe, K. Suzuki, and T. Takahashi, "Silica-Based PLC Transponder Aggregators for Colorless, Directionless, and Contentionless ROADM," OSA Optical Fiber Communication Conference (OFC), paper OTh3D.1 (2012).

[19] S. Nakamura, S. Yanagimachi, H. Takeshita, A. Tajima, "Optical Switches Based on Silicon Photonics for ROADM Application," IEEE Journal of Selected Topics in Quantum Electronics, vol. 22, issue 6, pp. 185-193 (2016).

[20] http://www.ieice.org/~pn/jpn/jpnm.html, accessed 1 February 2020.

[21] R. Inkret, A. Kuchar, and B. Mikac, "Advanced Infrastructure for Photonic Networks – Extended Final Report of COST Action 266," Faculty of Electrical Engineering and Computing, University of Zagreb (2003).

[22] Y. Mori, C. Zhang, and K. Kikuchi, "Novel Configuration of Finite-Impulse-Response Filters Tolerant to Carrier-Phase Fluctuations in Digital Coherent Optical Receivers for Higher-Order Quadrature Amplitude Modulation Signals," OSA Optics Express, vol. 20, issue 24, pp. 26236-26251 (2012).

[23] M. S. Faruk and S. J. Savory, "Digital Signal Processing for Coherent Transceivers Employing Multilevel Formats," IEEE/OSA Journal of Lightwave Technology, vol. 35, issue 5, pp. 1125-1141 (2017).

[24] D. Chang, F. Yu, Z. Xiao, N. Stojanovic, F. Hauske, Y. Cai, C. Xie, L. Li, X. Xu, and Q. Xiong, "LDPC Convolutional Codes Using Layered Decoding Algorithm for High Speed Coherent Optical Transmission," OSA Optical Fiber Communication Conference (OFC), paper OW1H.4 (2012).

[25] R. Shiraki, Y. Mori, H. Hasegawa, and K. Sato, "Design and Evaluation of Quasi-Nyquist WDM Networks Utilizing Widely Deployed Wavelength-Selective Switches," OSA Optics Express, vol. 27, issue 13, pp. 18549-18560 (2019).